INTERNATIONAL JOURNAL OF COMPUTERS COMMUNICATIONS & CONTROL
Online ISSN 1841-9844, ISSN-L 1841-9836, Volume: 20, Issue: 2, Month: April, Year: 2025
Article Number: 7027, https://doi.org/10.15837/ijccc.2025.2.7027

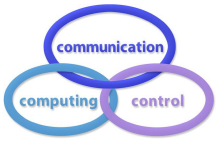

CCC Publications

NaturaSat computational tools for supporting hydrological modelling in environmental study and control

M. Kollár, I. Piačková, J. Papčo, M. Šibíková, J. Šibík, K. Mikula

Michal Kollár
Department of Mathematics and Descriptive Geometry
Faculty of Civil Engineering, Slovak University of Technology in Bratislava, Slovakia
michal.kollar@stuba.sk

Ivana Piačková
Department of Mathematics and Descriptive Geometry
Faculty of Civil Engineering, Slovak University of Technology in Bratislava, Slovakia
piackovai13@gmail.com

Juraj Papčo
Department of Theoretical Geodesy and Geoinformatics
Faculty of Civil Engineering, Slovak University of Technology in Bratislava, Slovakia
juraj.papco@stuba.sk

Mária Šibíková
Plant Science and Biodiversity Centre
Institute of Botany, Slovak Academy of Sciences, Slovakia
maria.sibikova@savba.sk

Jozef Šibík
Plant Science and Biodiversity Centre
Institute of Botany, Slovak Academy of Sciences, Slovakia
jozef.sibik@savba.sk

Karol Mikula*
Department of Mathematics and Descriptive Geometry
Faculty of Civil Engineering, Slovak University of Technology in Bratislava, Slovakia
*Corresponding author: karol.mikula@stuba.sk

Abstract

Wetlands, areas that are permanently or seasonally flooded or saturated with water, are among the most productive and biodiverse ecosystems on the planet. Their conservation, revitalization and health status monitoring require the hydrological modelling. We introduce the novel hydrological modelling tool in the NaturaSat software and show the useful workflows supporting environmental control and informed decisions. The tool is based on numerical solution of the Laplace equation with Dirichlet boundary conditions on a triangular grid using the complementary volume method. We present results for a case study of the Foráš Nature Reserve in Slovakia, in the alluvium of Danube River, demonstrating the practical application of developed methods. By comparing the solution with the Digital Terrain Model we study the waterlogging status of the most important wetland habitats in the area, and complement the results by analysis of Sentinel-1 radar satellite data and Sentinel-2 optical satellite data.

Keywords: software, image processing, image segmentation, numerical methods, hydrological modelling, satellite data, Sentinel-1, Sentinel-2

1 Introduction

Wetlands, defined as regions that are permanently or seasonally flooded or saturated with water, are among the most productive and diverse ecosystems on the planet. These unique ecosystems play a pivotal role in maintaining environmental balance and supporting life on Earth. They provide a range of vital ecosystem services essential to both the natural environment and human civilisation. Wetlands offer habitats for approximately 40% of the world's plant and animal species [9], serve as critical systems for water storage and purification, and help prevent erosion and control flooding. Despite their immense value, wetlands are under increasing threat due to human activities such as urban expansion, industrialisation, intensive agriculture, and deforestation, as well as the broader impacts of pollution and global climate change. This has resulted in a staggering loss of these vital ecosystems, with estimates suggesting that nearly 64-71% of global wetlands have disappeared since 1900 [5]. Preserving and restoring wetlands has therefore become an environmental priority, requiring comprehensive monitoring and analysis of their ecological health and hydrological status. Traditionally, the study and evaluation of wetlands have relied heavily on fieldwork, a process that is not only labour-intensive but also time-consuming and often spatially limited. While fieldwork remains an essential component of wetland research, recent advancements in geospatial technologies, remote sensing, and computational methods have opened new avenues for large-scale environmental analysis, offering efficient and innovative tools. Recognising these opportunities, our study seeks to contribute to ongoing efforts in wetland conservation by incorporating computational hydrological modelling into environmental research workflows. Specifically, we aim to enhance the capabilities of NaturaSat, an environmental software tool designed to support geobotanical and phytogeographical research using modern mathematical methods [16]. By integrating hydrological modelling techniques, we aim to provide researchers with tools for analysing wetland dynamics, assessing ecological conditions, and identifying areas in need of restoration. This paper presents an overview of the NaturaSat software, focusing on its numerical methods for image segmentation and its newly developed tools for computational hydrological modelling. These methodologies are then applied to a case study of a wetland area in Slovakia: the Foráš Nature Reserve. The analysis explores the geographical and historical significance of these sites and demonstrates the practical application of computational hydrological modelling, along with its validation using radar satellite data. Through this work, we aim to showcase the utility of integrating modern computational techniques into wetland research, empowering scientists and policymakers to make informed decisions regarding the preservation and restoration of these critical ecosystems.

2 NaturaSat software

The NaturaSat software is a large-scale system based on a multi-module architecture implemented in C++ [1]. The application is specifically designed for the Windows operating system, targeting the 64-bit platform. For the graphical user interface (GUI), the software utilizes the Qt widget toolkit (version 6.5.2), which is licensed under the LGPL v3 and GPL v3 open-source licenses. The system architecture prioritizes scalability and maintainability by applying modular design principles. This approach ensures that individual components can be developed, tested, and updated independently, facilitating future expansion and adaptability to evolving requirements. The modular architecture also enhances code reusability and reduces interdependencies between components, enabling robust software design. The GUI is designed to ensure user-friendliness, even for users without extensive knowledge of the complex methods or workflows employed by the software.

The flowchart in Figure 1 illustrates the workflow and interactions between tools and modules implemented in NaturaSat. The structured layout demonstrates how data flows through the system, from input to rendering and analysis. The user interface of NaturaSat is depicted in Figure 2.

The application offers an enhanced user experience by integrating several modules that provide intuitive interfaces and efficient data management. The Data Explorer is responsible for handling input-output file management, while the Data Renderer allows users to interact with visualized data through features such as zooming and panning. Georeferenced TIFF files, as well as images in standard formats like JPEG, PNG, GIF, and BMP, can be used as input data. This functionality enables

seamless loading of data representing Digital Terrain Models, historical maps, or orthophoto images into the software. For remote data access, the Remote Satellite Data Manager facilitates the download of Sentinel-2 satellite data via the Copernicus Data Space Ecosystem API. Additionally, by using the SNAP software the Sentinel-1 data can also be processed and loaded into the system [8] (see Section 3.2).

The following modules form the computational back-end of the software, providing capabilities for filtering, segmentation, monitoring, classification, hydrological modelling, and map transformation of areas of interest in data sources:

- Filtering Tool: Provides various filtering methods, including linear, nonlinear, and curvature diffusion, for pre-processing data sources.
- Semi-automatic Segmentation Tool: Supports the semi-automatic segmentation of areas of interest in processed data sources, assisting in identifying and delineating specific areas.
- Automatic Segmentation Tool: Automates the segmentation process for areas of interest in processed data sources, using algorithms to identify and segment areas without manual intervention.
- Monitoring Tool: Facilitates quality and area monitoring by analyzing and tracking changes in area conditions over time.
- Classification Tool: Performs classification of areas of interest using Natural Numerical Networks (NatNets) and generates relevancy maps.
- Hydrological Modelling Tool: Executes hydrological modelling for the area of interest.
- Historical Maps Transformation Tool: Helps users identify corresponding areas of interest on historical maps and the contemporary interactive map.

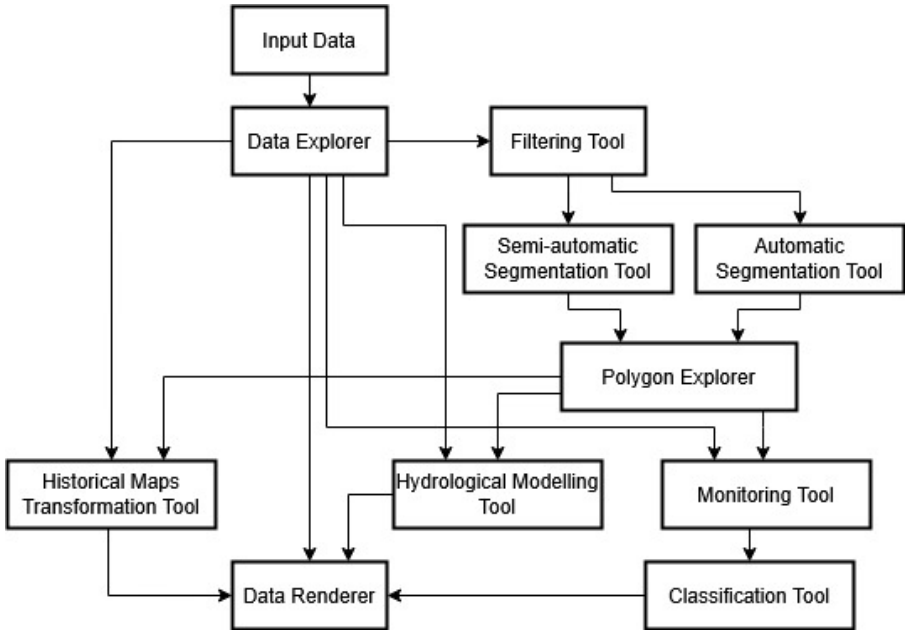

Figure 1: The flowchart demonstrates the interaction between modules and how data flows through the system, from input to rendering and analysis.

For the purposes of this paper, only a selection of modules related to the computational hydrological modelling will be discussed. A general overview of the software's usability can be found in [16]. For more information and examples of usage for the classification tools, refer to [17] and [18].

Figure 2: The user interface of the NaturaSat software with loaded Sentinel-2 data and highlighted segmentation polygons. *Data source: Sentinel-2 L2A product acquired on 14 August 2024 (Copernicus Data Space Ecosystem, ESA)*

2.1 Segmentation Tools

NaturaSat provides two segmentation methods: semi-automatic [14] and automatic segmentation models [15]. Both methods are based on a robust implementation of Lagrangian curve (we call it also polygon) evolution models, featuring tangential redistribution of evolving curve points and efficient handling of topological changes, such as the splitting and merging of evolving curves. The evolving curve is defined as $\Gamma : [0,T] \times [0,1] \to \mathbb{R}^2$, $\Gamma = \mathbf{x}(t,u)$, $t \in [0,T]$ is a time, $u \in [0,1]$ parametrize the curve, and $\mathbf{x}(t,u)$ represents the coordinates of polygon vertices during its time evolution. The general definition of curve evolution used in both models is $\mathbf{x}_t = \beta\mathbf{N} + \alpha\mathbf{T}$, where β represents the normal velocity, α represents the tangential velocity, $\mathbf{T}$ is the unit tangent vector to the arc-length parametrisation of the evolving curve, and $\mathbf{N} = \mathbf{T}^{\perp}$ is the unit normal vector. For semi-automatic segmentation, Γ is an open planar curve, and Dirichlet boundary conditions in the form $\mathbf{x}(t,0) = \mathbf{x}(0,0)$ and $\mathbf{x}(t,1) = \mathbf{x}(0,1)$, $t > 0$, are applied. Conversely, for automatic segmentation, Γ is a closed planar curve, and periodic boundary conditions in the form $\mathbf{x}(t,1) = \mathbf{x}(t,0)$, $t > 0$, are applied.

The semi-automatic segmentation method employs a normal velocity defined as

$$\beta = -\lambda(t)\nabla g_1(\mathbf{x}) \cdot \mathbf{N} - \delta(t)k(\mathbf{x},t).$$

In the case of the automatic segmentation, the normal velocity is expressed as

$$\beta = (1-\lambda(t))g_2(\mathbf{x}) - \lambda(t)\nabla g_1(\mathbf{x}) \cdot \mathbf{N} - \delta(t)g_2(\mathbf{x})k(\mathbf{x},t).$$

In both approaches, the normal velocity incorporates the function $g_1(\mathbf{x})$, which acts as an edge detector in the form

$$g_1(|\nabla \mathbf{I}^{\sigma}(\mathbf{x})|) = \frac{1}{1 + K\sum_{i=1}^{N}|\nabla I_i^{\sigma}(\mathbf{x})|^2}.$$

Here, $\mathbf{I}$ denotes the input image intensity vector consisting of optical channels I_i, $i = 1,\ldots,N$, while $\nabla\mathbf{I}^{\sigma}$ corresponds to the gradients of the filtered image data. The parameter σ specifies a strength of filtration, and K controls the sensitivity to the edges. The Filtering Tool module provides several diffusion- and curvature-based filtering techniques for preprocessing, including linear diffusion, the

regularized nonlinear Perona-Malik model, mean curvature flow, and geodesic mean curvature flow. The term $-\nabla g_1(\mathbf{x})$ defines a vector field that directs the evolving curve precisely toward the edges representing boundary of the segmented region. In automatic segmentation, the normal velocity contains also the function $g_2(\mathbf{x})$. This term guides the segmentation curve from its initial position, through the region of interest, to its boundary. The expanding behavior is expressed as $g_2(\mathbf{x}) = H(\mathbf{x})g_1(\mathbf{x})$, where $H(\mathbf{x})$ operates as the homogeneity function, identifying whether $\mathbf{x}$ lies within the segmented region. This homogeneity function is based on statistical features, such as the mean, minimum, or maximum, calculated from image data inside the initial curve. The parameter $\lambda(t)$ weights the edge-attracting vector field and the expansion velocity in the normal direction. Due to noise and smoothness requirements, the last term in the normal velocity for both segmentation models includes the curvature term. This term ensures that the curve evolution is regularized by the curve curvature $k(\mathbf{x}, t)$, while $\delta(t)$ weights the influence of the curvature as time evolves. For automatic segmentation, the term is further influenced by the function $g_2(\mathbf{x})$, which modulates the curvature smoothing effect near the border of the segmented region. Lastly, to redistribute the points along the curve, the models include the asymptotically uniform tangential redistribution driven by the tangential velocity α [20]. This tangential redistribution prevents the numerically evolving curve from self-intersections and other singularities, while also enabling the fast detection and resolution of topological changes [2].

The evolution is solved using the flowing finite volume method, combining a semi-implicit scheme for the diffusion term with an inflow-implicit/outflow-explicit strategy for the intrinsic advection term [2]. For semi-automatic segmentation, an efficient gradient-driven initial condition is applied. This condition ensures that the initial position of the evolving curve is near the boundary of the segmented object, resulting in improved performance for real-time segmentation [3].

2.2 Computational hydrological modelling

Computational hydrological modelling is performed by a module implemented in the NaturaSat software. We consider the groundwater and free water table surface to behave like an elastic membrane connecting boundary conditions, which can be described using a non-linear minimal surface equation. To solve this, we use the Laplace equation, as it serves as a standard approximation of the minimal surface equation in cases where the solution's gradients are small. We also assume that the porous medium for groundwater flow is homogeneous. The primary objective of hydrological modelling is to determine the water level, i.e. the free water table interconnected with the groundwater table represented by the upper boundary of the saturated zone, within a selected computational region. The boundary of this region is defined by a segmentation polygon, which can be obtained through semi-automatic or automatic segmentation module available in NaturaSat (see 2.1). On the boundary of the region, we impose Dirichlet boundary conditions, representing the water level at specific vertices of the segmentation polygon.

To solve this boundary value problem, we apply the complementary volume method on an irregular triangular grid [11]. First, we discretize the computational region into a triangular grid by triangulating the polygonal region using the CGAL library [4]. Several types of triangulations can be chosen for solving this boundary value problem. In our case, we focus on Delaunay triangulation, specifically constrained Delaunay triangulation, because it produces acute triangles of similar size and shape. Constrained triangulation is a type of triangulation that enforces specific polylines to be included among the resulting edges of created triangles. These polylines are referred to as *constraints*, and the corresponding edges in the triangulation are called *constrained edges*. This type of triangulation aligns with our objectives, as we aim to create a primal triangular grid over the area bounded by a segmentation polygon respecting its line segments within the grid.

The Laplace equation is a second-order partial differential equation given by

$$-\Delta u(x) = 0, x \in \Omega,$$

where Δ represents the Laplace operator, u is a twice-differentiable function, and Ω is the domain in which the equation is solved. In our case, Ω corresponds to the region bounded by the segmentation polygon. When Ω is a bounded region, solving the equation requires specifying boundary conditions

$u(x) = u_D(x), x \in \partial\Omega$, where $u_D(x)$ is a given function and $\partial\Omega$ is the boundary of Ω. The Laplace equation is numerically solved using the complementary volume method, which results in a system of linear equations where the unknowns represent the water levels at the nodes of the generated triangulation. This system is solved using the BiCGSTAB (biconjugate gradient stabilized) method, an iterative solver specifically designed for sparse square matrix problems.

To visualize the solution defined at the vertices of the triangular grid within the NaturaSat software, the solution is interpolated onto a regular rectangular grid using the scan-line algorithm for polygon filling and barycentric interpolation. This rectangular grid must encompass the entire region bounded by the segmentation polygon, serving as its rectangular hull. Pixels outside this region are assigned the minimum value, corresponding to black color in the created image. Conversely, pixels within the triangles or along their edges in the triangular grid are assigned colors from a gradient defined by an RGB color transfer function (see Figure 11).

Information about the water level within the region of interest is not sufficient on its own for computational hydrological modelling. We are particularly interested in the relationship between the water surface and the ground surface. To compare the water level with the ground elevation, we use Digital Terrain Model (DTM) data (see 3.1) within the region of interest. The DTM contains ground elevation data derived from a classified point cloud obtained through airborne laser scanning (ALS). For water bodies, the data represents the elevation of the water surface at the time of scanning, interpolated from points on the water surface and along the shore. The solution to the Laplace equation is computed and then interpolated onto a rectangular grid at a resolution matching that of the DTM, similarly to its visualization described above. The height differences between the solution of hydrological modelling and the DTM indicate whether the water level is below/on/above the ground surface in the area of interest under the specified boundary conditions. The entire workflow of the designed methodology is illustrated in Figure 3.

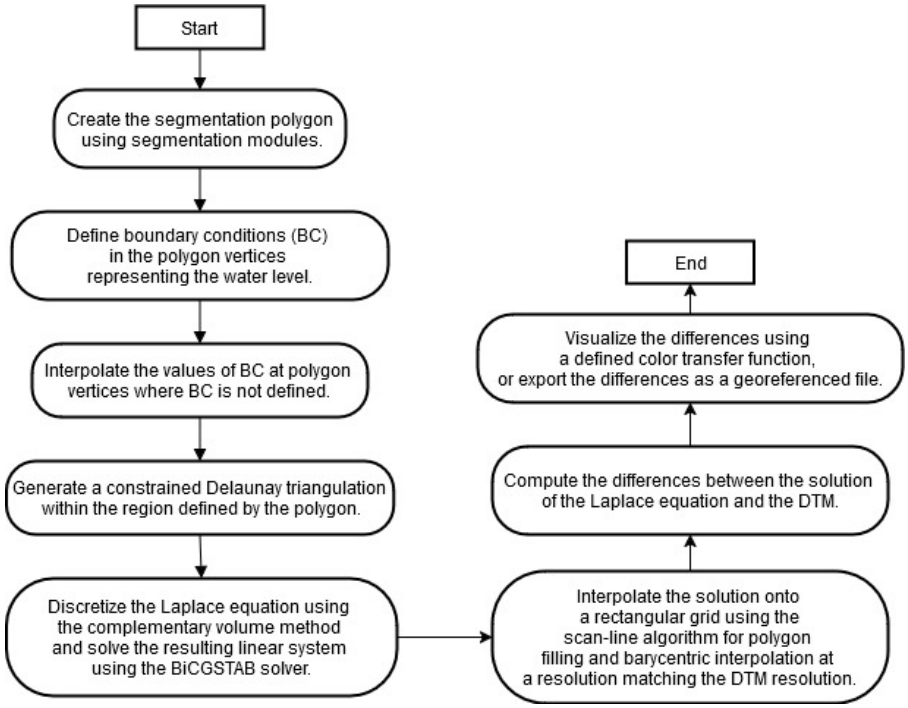

Figure 3: The workflow of the designed methodology for the computational hydrological modelling.

3 Input data

3.1 Digital Terrain Models

Since 2022, the Geodesy, Cartography, and Cadastre Authority of the Slovak Republic (ÚGKK SR) has been updating the Airborne Laser Scanning (ALS) products as part of the second cycle of ALS

data collection in selected parts of Slovakia. The first cycle (2017–2023) resulted in the creation of the Digital Terrain Model 5.0 (DTM 5.0) for the entire territory of Slovakia with a resolution of 1×1 m. The Digital Terrain Model 6.0 (DTM 6.0), the newest product, offers a resolution of 0.5×0.5 m and is currently available for six already processed localities (lots), including our region of interest [7]. DTM 6.0 was generated by interpolation from classified point clouds provided by ALS, using classification class 02 Ground as the input. The scanning was performed during the vegetation-free winter period (from October 15 to April 15), and the resulting DTM is available as georeferenced TIFF files, which can be loaded directly into NaturaSat. The vertical accuracy of point clouds in the second cycle is ≤ 0.1 m, and the positional accuracy is ≤ 0.2 m [6]. However, in areas with low reflectance, such as water bodies, the density of points in the point cloud is lower. This can result in the elevation within water bodies being interpolated from elevation points along the shore. This issue will be discussed further in Section 4.2. A visualization of DTM 6.0 is provided in Figure 9.

3.2 Sentinel-1

The flooding or presence of water in a selected region can be effectively observed using Sentinel-1 data. Sentinel-1 is a radar imaging satellite mission operated by the European Space Agency (ESA) as part of the Copernicus Program [22]. Its Synthetic Aperture Radar (SAR) technology offers the advantage of operating at wavelengths that are unaffected by cloud cover or the absence of illumination, enabling data acquisition during both day and night under all weather conditions. Specifically, Sentinel-1 Ground Range Detected (GRD) products are pre-processed radar datasets in which detected amplitude values are projected to ground range using an Earth ellipsoid model. GRD products are widely utilized for applications such as land cover mapping, flood monitoring, and surface deformation analysis due to their spatial resolution (ranging from 10 to 40 meters) and consistent temporal coverage. These datasets are freely available and can be accessed through the Copernicus Data Space Ecosystem [10].

Sentinel-1 GRD products include dual-polarization data, specifically VV (vertical transmit and vertical receive) and VH (vertical transmit and horizontal receive) polarizations. These polarizations provide complementary information about the Earth's surface. The VV polarization mode is particularly sensitive to smooth surfaces, such as calm water bodies, making it effective for detecting open water[22].

To process Sentinel-1 data in NaturaSat, it is necessary to preprocess the data in the SNAP application using the Sentinel Toolboxes provided by the ESA [8]. The software includes the Graph Builder component, which is used for batch processing of Sentinel-1 data. Figure 4 illustrates the graph workflow designed in the Graph Builder component. Each dataset follows the same workflow, consisting of the following steps [12]:

1. Apply Orbit File - This step ensures accurate satellite position information.
2. Thermal Noise Removal - This step removes thermal noise from the GRD data.
3. Calibration - This step converts the digital numbers to backscatter values.
4. Terrain Correction - This step corrects geometric distortions caused by terrain effects.
5. Conversion to dB - Sentinel-1 backscatter values are typically in power units. Converting to decibels (dB) compresses the dynamic range and improves visualization.
6. Export to TIFF File - To load data into NaturaSat, the data needs to be exported as a TIFF file with with georeferencig to the selected projection like UTM.

3.3 Sentinel-2

Monitoring flooding or water presence in a specific region can also be supported using Sentinel-2 data. Sentinel-2 is an optical imaging satellite mission operated by the ESA under the Copernicus Programme [23]. It provides high-resolution multispectral imagery across 13 spectral bands, spanning

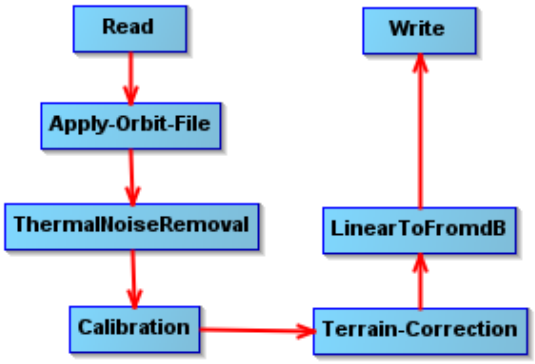

Figure 4: The graph workflow designed in the Graph Builder component of SNAP v11.0.0 software.

visible, near-infrared (NIR), and shortwave infrared (SWIR) wavelengths. This capability enables detailed observation of land and water surfaces, making Sentinel-2 particularly valuable for applications such as flood mapping, water quality assessment, and vegetation monitoring. Sentinel-2's MultiSpectral Instrument (MSI) captures data at spatial resolutions of 10 m, 20 m, and 60 m, depending on the spectral band. The mission's twin satellites, Sentinel-2A and Sentinel-2B, operate in a sun-synchronous orbit, phased 180° apart, ensuring global coverage with a revisit time of five days at the equator. This high temporal resolution allows for the frequent monitoring of dynamic phenomena, such as changes in water extent during floods or seasonal variations in vegetation and soil moisture [23].

A key feature of Sentinel-2 is its ability to distinguish between water bodies and other land cover types using specific spectral bands. For instance, the NIR and SWIR bands are highly sensitive to water content, making them effective for detecting water surfaces and assessing soil moisture levels. Particularly, Gao's Normalized Difference Water Index (NDWI) can detect moisture levels in vegetation by combining NIR and SWIR spectral bands [13]. Sentinel-2 data is freely accessible through the Copernicus Data Space Ecosystem. An example of Sentinel-2 data loaded into the NaturaSat software, specifically the RGB optical bands, can be seen in Figure 2.

4 Computational hydrological modelling in the Foráš Nature Reserve area

4.1 Geographic and historical context

The site, approximately 2×2 km in size, is located within the Danube River alluvium, bordered by the branches of Bodícke Rameno, and is part of an active inundation zone, consequently influenced by the river's hydrological regime. The geological basement is composed of gravel-sand deposits. The site lies between the artificial channel of the Danube, which flows to the Gabčíkovo hydropower plant, and the old Danube River stream (see Figure 5).

The branch system of the Danube River has changed significantly over time in the target area. On the maps of the First and Second Military Surveys [24] [25], it was impossible to identify branch structures similar to those of today. However, on the Third Military Survey [26], the branch system becomes recognizable and comparable to the present one (see Figure 6). The Third Military Survey of the Habsburg Empire (conducted from 1869 to 1887 and completed before and during the first years of the First World War) provides a detailed cartographic description of the Austro-Hungarian state at the end of the 19th and the beginning of the 20th century. It includes a precise cartographic depiction of the Danube River region along the present-day Slovakia–Hungary border.

The historical river branch system was semi-automatically segmented using the segmentation mod-

Figure 5: Danube branch system around the Bodícke Rameno. The area, approximately 2×2 km in size, where the Foráš Nature Reserve is located, and which is used for computational hydrological modelling is marked with a red square. *Data source: Orthophotomosaic of Slovakia from 2023(GKÚ Bratislava, NLC).*

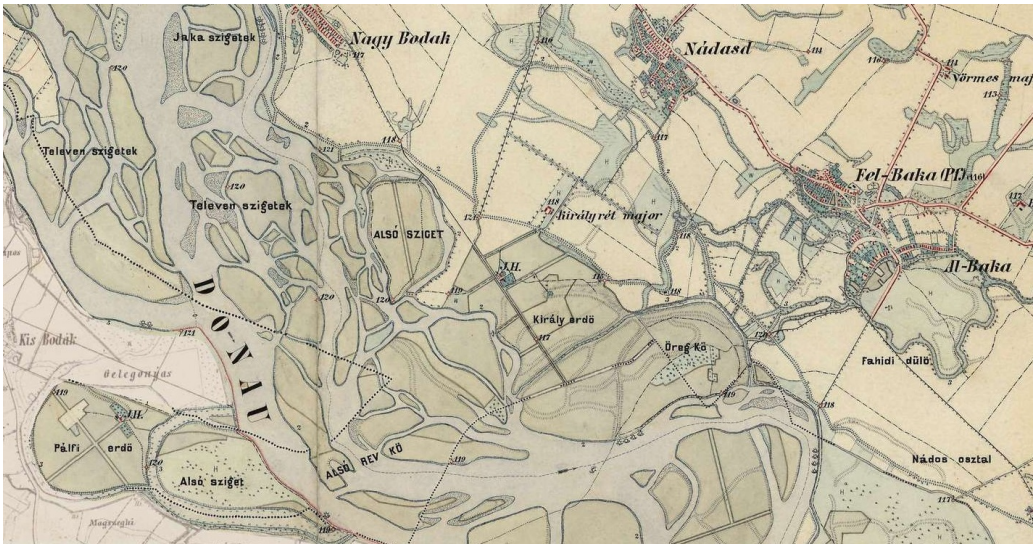

Figure 6: The Danube branch system around the Bodícke Rameno as depicted on historical maps from the Third Military Survey. *Data source: Historical map of III. military survey in raster form (GKÚ Bratislava, NLC).*

ule (see Section 2.1) on the map of the Third Military Survey. It was then transformed into the contemporary OpenStreetMap [21] using the NaturaSat Historical Maps Transformation module, which employs the Locally Affine Globally Laplace (LAGL) algorithm [19] (see Figure 7), and superimposed with Sentinel-2 and Orthophotomosaic images (see Figure 8). This analysis reveals shifts in the borders of historical islands within the branches, indicating that the branch system was more complex in the past. Remnants of historical streams are clearly visible within the Foráš nature reserve (south-east part of our computational domain), and the most ecologically valuable part of the reserve corresponds to the island located between the streams at the lower middle part of the historical branch system.

Figure 7: The segmentation of a part of the Danube branch system around the Bodícke Rameno performed on historical maps from the Third Military Survey (left), transformed to OpenStreetMap using the LAGL algorithm [19] (right). *Data source: Historical map of the Third Military Survey in raster form (GKÚ Bratislava, NLC) and OpenStreetMap.*

Figure 8: The transformed segmentation of a part of the Danube branch system around the Bodícke Rameno is positioned over Sentinel-2 data (left) and an orthophotomosaic image (right). *Data source: Sentinel-2 L2A product acquired on 30 July 2024 (Copernicus Data Space Ecosystem, ESA) and Orthophotomosaic of Slovakia from 2020 (GKÚ Bratislava, NLC).*

4.2 Results

For the computational hydrological modelling in the Foráš Nature Reserve area, we used two different sets of input data representing boundary conditions. The first dataset consists of water level values from DTM 6.0 (see Section 3.1), while the second includes water level values obtained directly in the field through continuous measurements using a precise geodetic GNSS antenna operated from a boat.

In the DTM 6.0 data with a resolution of 0.5×0.5 m, we semi-automatically segmented the region of interest (see Figure 9, red curve). As we need the boundary of the computational domain to be located approximately in the middle of the surrounding distributaries, this polygon serves as the initial curve for automatic segmentation algorithm performing several steps of polygon dilation. Using the parameters $\lambda = 0$ and $g_2 = 1$ in the normal velocity for automatic segmentation, this initial curve is evolved in the normal direction for specific time steps. In this case, since the narrowest width of the surrounding distributaries is approximately 40 m, we evolved the initial curve by 20 m toward the centerlines of distributaries (see Figure 9, blue curves). The final polygon will be used to define the boundary of computational domain for hydrological modelling.

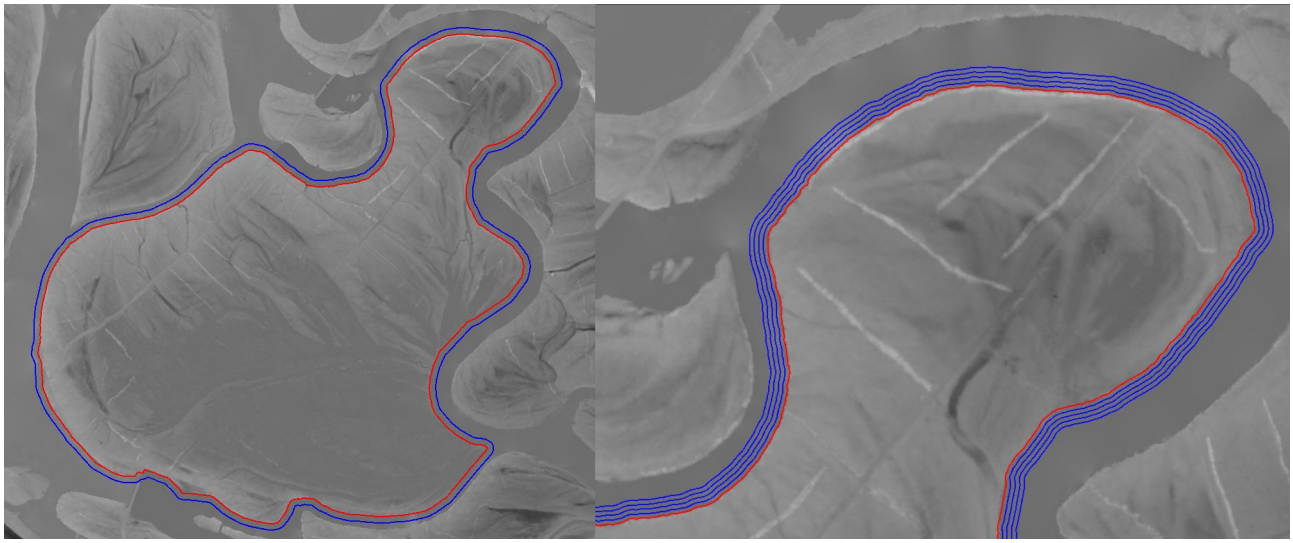

Figure 9: The red segmentation polygon represents the semi-automatically segmented area of interest on the DTM 6.0 data, while the blue polygons show the results of the automatic segmentation algorithm performing dilation of the curve. In the left image, only the final step is displayed, showing the initial polygon shifted approximately 20 m from the shore toward the distributaries. The right image provides a detailed view of the northern area, where multiple steps of the automatic segmentation are visible, with each step showing a shift of 5 m. *Data source: DTM 6.0 from 2022 (GKÚ Bratislava).*

To reduce the computational complexity of hydrological modelling, we coarsen the discretization of the polygon and define the computational domain so that the average arc-length distance between two polygon points is approximately 25 m (see Figure 10). As briefly mentioned in Section 3.1, the DTM in the distributaries is interpolated from elevation points obtained from the point cloud also along the shores. This can cause sudden elevation changes in the distributaries due to interpolation errors. Therefore, the boundary condition from the DTM data will not be set at every vertex of the polygon but only at those where the DTM values satisfy $|u(\mathbf{x}(i)) - u(\mathbf{x}(i-1))| \leq 0.1$ m and $|u(\mathbf{x}(i)) - u(\mathbf{x}(i+1))| \leq 0.1$ m for $i = 0, \ldots, N$, where N is the number of polygon vertices, and $u(\mathbf{x}(i))$ is the DTM value of the pixel associated with the polygon point $\mathbf{x}(i)$ (see Figure 10). The values at the remaining vertices of the polygon are determined by interpolating the values from the vertices with defined boundary conditions. The values at polygon vertices represent the water levels on the day of the ALS, which for this area occurred between November 30 and December 1, 2022, and their range is [117.146, 117.771] meters. In Figure 11 (left), the solution of the hydrological modelling, where the boundary conditions are obtained from the DTM, is depicted. We observe that the highest water level occurs in the western part of the region, while the lowest is in the east. This result is expected, as

two weirs located within the distributaries reduce the water level by a few tens of centimetres.

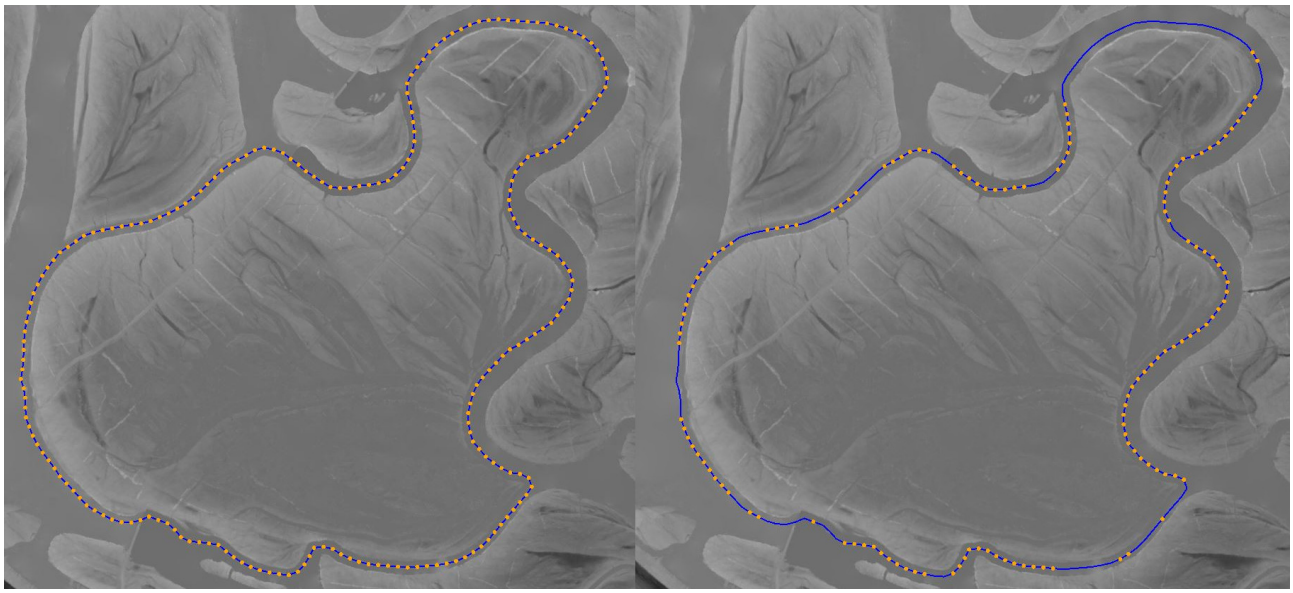

Figure 10: All vertices of the polygon defining the computational domain boundary (left), and only those where the boundary condition from DTM 6.0 is applied (right). *Data source: DTM 6.0 from 2022 (GKÚ Bratislava).*

The most important wetland habitat types in the area were segmented semi-automatically using orthophotomosaic images and subsequently verified in the field by botanists. The following habitats were identified:

- 91E0 Willow-poplar floodplain forests – This habitat is characterized by areas that should be flooded or partially flooded for a certain period (1–2 months per year) (see Figure 12).
- Lk11 Reed beds – This habitat occurs under conditions where the water table fluctuates between a few centimeters below the ground surface and up to 0.5 meters above it.
- 3150 Natural eutrophic lakes with Magnopotamion or Hydrocharition-type vegetation – This habitat requires the presence of a water table throughout the year, although it may temporarily dry out for a few weeks.

The differences between the solution of the hydrological modelling and the DTM are calculated and depicted in Figure 11 (right). In these images, blue regions represent areas where the computed water surface is more than 20 cm above the ground, while red regions indicate areas where the water surface is more than 20 cm below the ground. White regions correspond to areas where the solution of the hydrological modelling is close to the DTM. The threshold plus/minus 20 cm is related to the accuracy of DTM in our region of interest. In relatively flat subregions of our domain, we computed the maximum height difference in the DTM over a 20 cm distance (which is the positional accuracy of the DTM) and found out that it is approximately 10 cm. Adding this to 10 cm vertical accuracy of the point cloud data we arrive to the considered threshold. This leads to the conclusion that white areas of the image indicate the presence of a free water table or saturated groundwater table. In Figure 11 (right), the polygons of the most important wetland habitats are also plotted. As we can see, the distribution of habitats aligns well with their environmental requirements, although in certain areas, the water level is insufficient. Purple polygons represent 91E0 Willow-poplar floodplain forests - habitat that should be flooded or partially flooded for some time. Within these polygons, white areas are predominantly visible. The only exception is a habitat polygon in the northern part of the area, which represents a 91E0 forest in unfavorable condition (visible as a strong red color). Black polygons represent Lk11 Reed beds, which occur in conditions where the water table is approximately at the terrain level, except the east ones. Green polygons correspond to 3150 Natural eutrophic

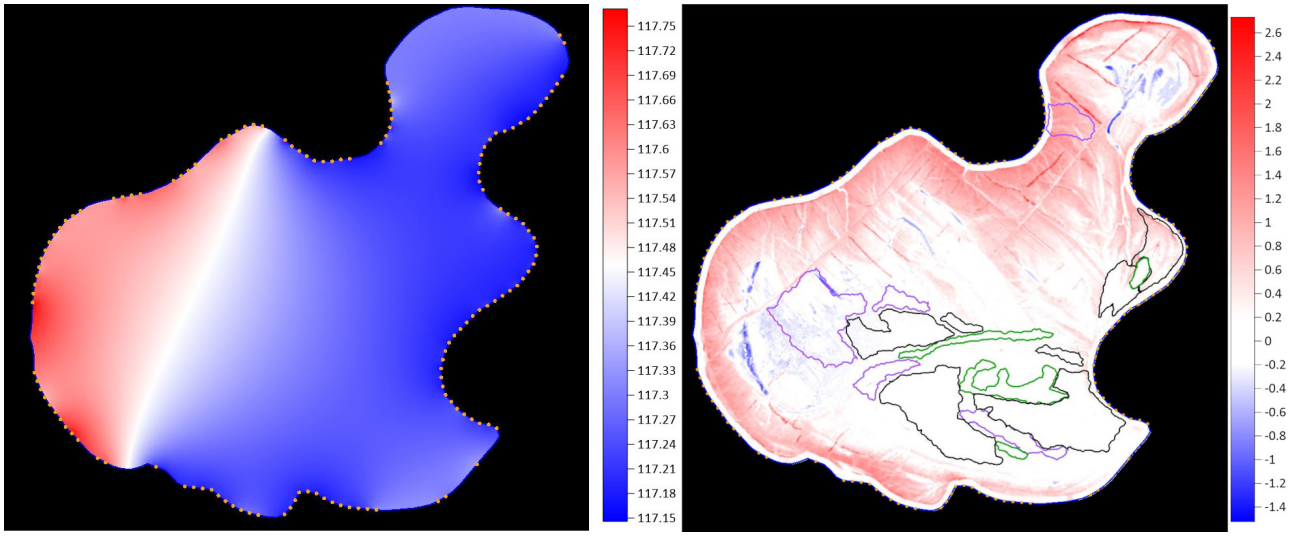

Figure 11: The solution of the hydrological modelling with boundary conditions obtained from the DTM (left). Red areas represent the maximum value of 117.771 meters, while blue areas correspond to the minimum value of 117.146 meters. The differences between the solution of the hydrological modelling and the DTM, along with polygons representing the most important wetland habitats (right). Purple polygons represent 91E0 Willow-poplar floodplain forests, black polygons represent Lk11 Reed beds, and green polygons correspond to 3150 Natural eutrophic lakes with Magnopotamion or Hydrocharition-type vegetation. Both scales are in metres.

lakes with Magnopotamion or Hydrocharition-type vegetation and differences within these polygons clearly confirm the presence of water table. We should also note that theoretically there should not be any blue region in this experiment when we prescribe the boundary conditions from the same date as ALS was performed. As we see, some small percentage of the area is blue which is caused by inhomogeneity of porous media at those parts of the domain, e.g., presence of narrow forest roads visible in orthophotomosaics or other natural or artificial barriers that may disturb the otherwise homogeneous environment and block the natural flow of water. When solving the Laplace equation we have to accept this modelling error which is however not critical even in this example. Moreover, when using real or simulated boundary conditions higher than DTM on the domain boundary, the presence of blue regions is perfectly justified because in that case the water can be above the cloud points representing the terrain. That will be the case of the next experiments related to artificial controlled flooding and computer simulated flooding of the area.

Figure 12: Willow-poplar floodplain forests forest during artificial flooding (left) compared to the same forest in summer with low water levels (right).

As the second set of input data, we used water level values obtained directly in the field at the time of artificial flooding, on March 14, 2024, through continuous measurements with a precise geodetic GNSS antenna operated from a boat. For precise water level height determination, the network-based correction service SKPOS and the satellite-based correction service Trimble RTX were utilised. The Bodícke Rameno branch is part of the so-called Danube inland delta - an area of Danube branches, oxbows, and wetlands formerly nourished by Danube water. Since the construction of the Gabčíkovo hydroelectric power plant, the area has been connected to the Danube water only through an artificial supply system, and artificial floods are now the only significant way to replenish it. The spring 2024 artificial flood is the ninth consecutive flood of the branch system, which, like all previous ones, is the result of extensive negotiations between conservationists, water managers, and energy companies. The flow was gradually increased over a few days, culminating on March 14 at a maximum discharge of 120 m^3/s, which was directed into the territory over the following 15 days. During this period, wetlands were filled with water, floodplain forests were flooded, and the increased flow helped flush sediments from river branches, exposing the gravel bed and improving water infiltration into the subsoil.

Using a precise geodetic GNSS antenna operated from a boat, we recorded elevation values along the boat's trajectory. This dataset includes GPS coordinates for each measurement. In Figure 13 (left), the trajectory is shown. Using the Adjust function from the NaturaSat segmentation tool, the trajectory polygon was slightly smoothed to reduce topological anomalies along the boundary of the computational domain. Additionally, we reduced the density of vertices in the polygon to improve computational efficiency. The values for the new vertices of the adjusted polygon were obtained using nearest-neighbor interpolation from the original field measurements. The orange dots in Figure 13 (left) represent the vertices with boundary conditions. Notably, in the area of the weirs, the orange dots are absent because the boat with the measurement device cannot traverse these areas and must be transported by land; thus, measurements from this region are missing.

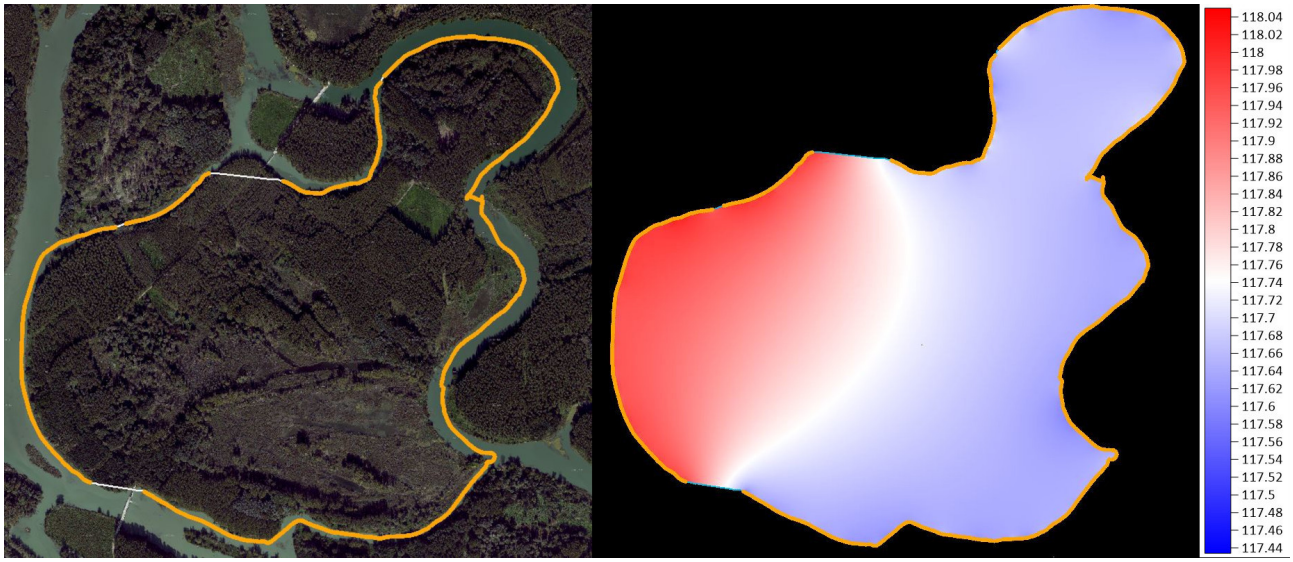

Figure 13: The smoothed boat GPS trajectory, with orange points representing the vertices at which boundary conditions, in the form of water levels recorded by a precise geodetic GNSS antenna, are applied (left). *Data source: Orthophotomosaic of Slovakia from 2020 (GKÚ Bratislava, NLC).* On the right, the solution of the hydrological modelling is presented, based on boundary conditions obtained using the precise geodetic GNSS antenna, where red represents the maximum value of 118.05 meters and blue corresponds to the minimum value of 117.434 meters. The scale is in metres.

In Figure 13 (right), the solution of the hydrological modelling is presented. Similar to the scenario where boundary conditions were derived from the DTM, the highest water levels occur in the western part of the region, while the lowest levels are situated in the east. In this case, water levels are approximately 0.4 meters higher because the branch flow during the time of measurement coincided with the artificial flood in the Danube River branches, resulting in measurements exceeding those taken during the ALS survey. In Figure 14 (left), a comparison between the DTM and the solution

of hydrological modelling is depicted. As shown in the figure, the extent of the artificial flooding was sufficient to inundate all segmented habitats, except for the 91E0 forest in the north (in unfavorable condition) and a small section of the eastern reed beds.

Using the first dataset, which consists of elevation values from DTM 6.0, and by increasing the water level values in the boundary conditions, we can computationally simulate scenarios of controlled flooding. These scenarios involve rising water levels in the surrounding distributaries, enabling us to identify areas that could theoretically be flooded. In Figure 14 (right), the differences between the results of hydrological modelling and the DTM are shown when boundary conditions increased by 40 centimeters are applied. These differences align with those observed in a scenario where boundary conditions were derived from precise geodetic GNSS measurements taken from a boat. This suggests that the results of hydrological modelling, adjusted using DTM boundary data with expected water increase level, can serve as an efficient alternative to in-field measurements, which are typically more time-consuming and costly. This leads to the conclusion that the workflow shown in Figure 3 can be used to determine the necessary water level increase required to maintain wetlands in a healthy state or to create conditions favorable for wetland revitalization.

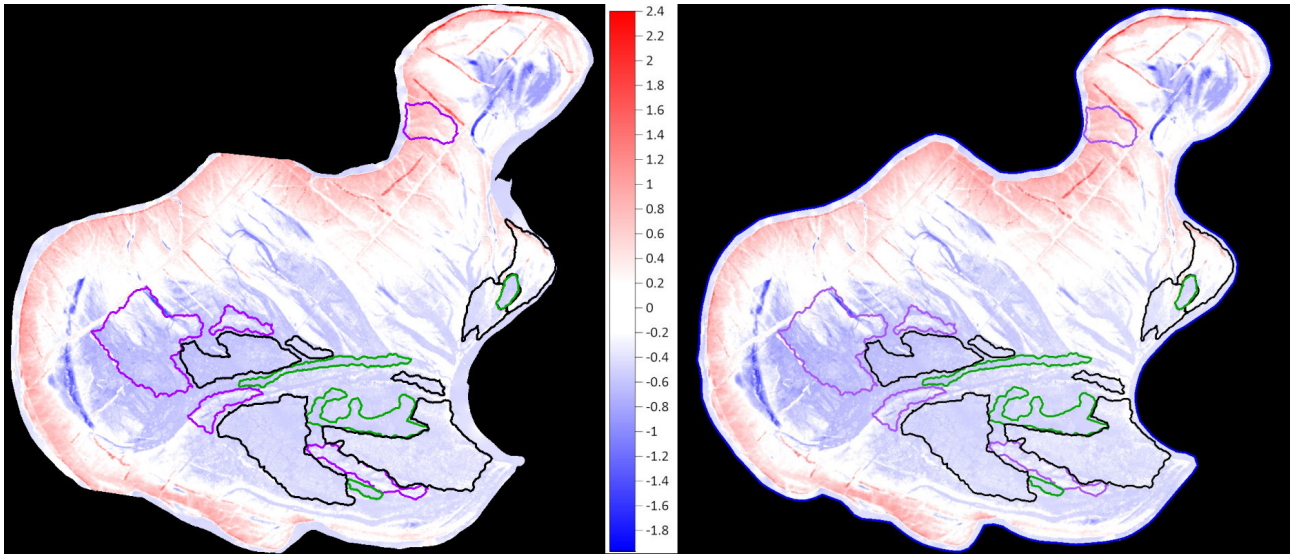

Figure 14: Differences between the hydrological modelling solution and the DTM using boundary conditions derived from in-field measurements (left), and, differences of the hydrological modelling solution and the DTM using raised boundary conditions from the DTM, representing increased water levels in the surrounding distributaries by 0.4 m (right). The scale is in metres.

To complement the results of the hydrological modelling, we can use Sentinel-1 data, as the flooding of the selected region can also be observed in this dataset. For this purpose, we downloaded two Sentinel-1 Level-1 GRD datasets from the Copernicus Data Space Ecosystem and preprocessed them using SNAP software (see Section 3.2). The first dataset is from December 3, 2022, which corresponds approximately to the time when the input point cloud data from ALS was collected for the DTM. The second dataset is from March 15, 2024, as this date is closest to when the field research was conducted to measure water levels using a precise geodetic GNSS antenna. In Figure 15, the Sentinel-1 VV polarization data, converted to decibels, from the region are displayed. As shown, the flooding on March 15, 2024, is clearly visible, as VV polarization consists of smaller values (indicated by black pixels). Smaller values in Sentinel-1 data, particularly on the decibel scale, typically indicate smoother surfaces with less backscatter, which suggests the presence of water or flooded areas. This occurs because water surfaces tend to reflect radar signals away from the satellite, resulting in lower backscatter values and causing flooded regions to appear darker in the imagery.

To compare these two datasets, we computed by NaturaSat monitoring tool statistical features (mean and minimum) for Sentinel-1 VV polarization data within the polygon representing boundary of the computational region (see Table 1). The mean values provide an overall representation of the backscatter across the region, while the minimum values highlight areas with the least backscatter,

often corresponding to more consistently flooded areas. The values in Table 1 show that both the mean and minimum features are lower in the data from March 15, 2024, which aligns with the flooded status of the region. The differences are particularly noticeable in the statistics from the habitat 3150 Natural eutrophic lakes with Magnopotamion or Hydrocharition-type vegetation (see green polygons in Figure 14). Table 2 presents the statistical features for four segmented regions of this habitat. These statistics clearly indicate that the Sentinel-1 data from March 15, 2024, exhibit significantly lower values, suggesting a greater presence of water in these lake habitats compared to the data from December 3, 2022. Lower decibel values in the March 15, 2024, dataset reflect higher water coverage in the habitats, confirming the effectiveness of the artificial flooding in sustaining these lake ecosystems.

	Mean	**Min**
December 3, 2022	-9.3801	-21.1829
March 15, 2024	-9.56918	-30.9521
Differences	-0.18908	-9.7692

Table 1: Statistical features (mean and minimum) computed from Sentinel-1 GRD VV polarization data converted to decibels from two different periods for the whole region. All values are in decibels.

Curve Name	**December 3, 2022**		**March 15, 2024**		**Difference**	
	Mean	Min	Mean	Min	Mean	Min
curve_3150_1	-11.7593	-19.2573	-13.1881	-19.2535	-1.4288	0.0038
curve_3150_2	-13.8528	-18.8685	-16.4891	-22.7428	-2.6363	-3.8743
curve_3150_3	-9.96913	-14.4996	-11.9903	-17.788	-2.02117	-3.2884
curve_3150_4	-11.6395	-21.1829	-19.0074	-30.9521	-7.3679	-9.7692

Table 2: Statistical features (mean and minimum) computed from Sentinel-1 GRD VV polarization data (converted to decibels) for two different periods, for segmented regions of habitat 3150 – Natural eutrophic lakes with Magnopotamion or Hydrocharition-type vegetation. All values are in decibels.

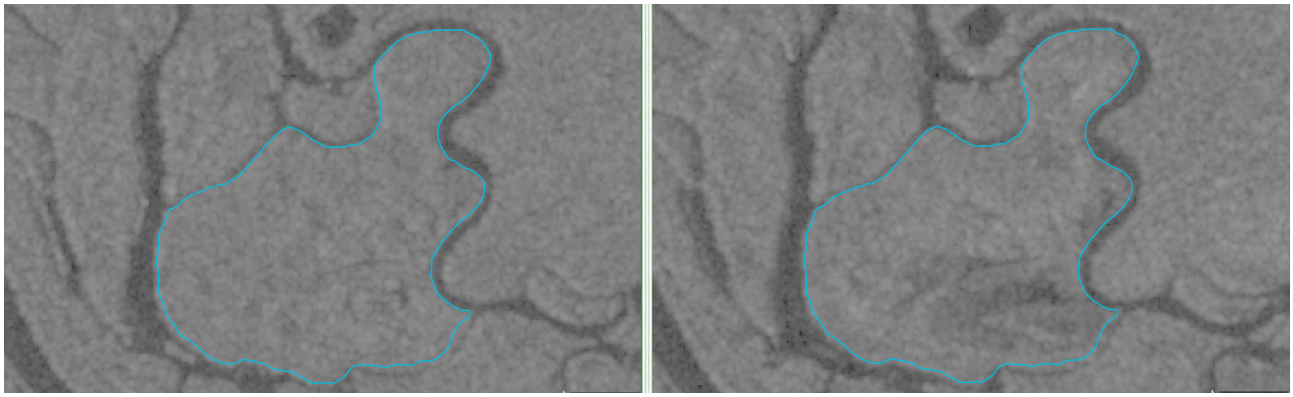

Figure 15: Sentinel-1 GRD data (VV polarization) converted to decibels from two different periods: December 3, 2022 (left), and March 15, 2024 (right).

Sentinel-1 data are useful for detecting increases in open water habitats, such as the 3150 Natural eutrophic lakes with Magnopotamion or Hydrocharition-type vegetation habitat. However, to detect moisture levels in vegetated habitats, Sentinel-2 optical data are more suitable. We downloaded Sentinel-2 Level-2A datasets using the Remote Satellite Data Manager in the NaturaSat software for two dates. The first dataset is from December 13, 2022, while the second is from March 17, 2024, which is the date closest to the artificial flood in the branch system. The monitoring tools within the software allow us to compute statistical features (mean, minimum and maximum) of Gao's NDWI (Normalized Difference Water Index) , defined as $\text{NDWI} = (\text{NIR}_{\text{B8}} - \text{SWIR}_{\text{B12}})/(\text{NIR}_{\text{B8}} + \text{SWIR}_{\text{B12}})$, where NIR_{B8} is the near-infrared B8 optical channel, and SWIR_{B12} is the shortwave infrared B12 optical channel. The index ranges from -1 to +1, where lower values indicate low vegetation water content, and higher

values correspond to higher water content. A decrease in Gao's NDWI suggests water stress, while high index values may signal waterlogging.

The specific thresholds for Gao's NDWI can vary depending on factors such as vegetation density, soil type, and atmospheric conditions. It is therefore essential to calibrate these thresholds for the specific study area and conditions using ground truth data to ensure accurate assessments of varying water levels. Commonly used threshold values are often calibrated for crop fields; however, in our case, we monitored wetland vegetation with specific water requirements. During field monitoring, we confirmed that positive NDWI values generally indicate a good water supply for wetland plants, while values above 0.1 indicate waterlogging.

The visualisation of Gao's NDWI for both dates is shown in Figure 16. In the figure, the segmentation curves of the most important wetland habitats in the area are also visible. The statistical features for the segmentation curves of 91E0 Willow-poplar floodplain forests and Lk11 Reed beds habitats, computed from Gao's NDWI, are presented in Table 3. As observed, mean, minimum and maximum values for each of the selected habitats are higher in the March 2024 dataset, successfully detecting the artificial flooding performed on the river branches. Moreover, the mean values are greater than 0.1, which corresponds to a high water supply and waterlogging. Since Gao's NDWI indicates vegetation water content, it is less effective for detecting changes in open water habitats such as the 3150 Natural eutrophic lakes with Magnopotamion or Hydrocharition-type vegetation habitat. For this type of habitat, using Sentinel-1 data is more suitable for detecting water-level increases (see Table 2).

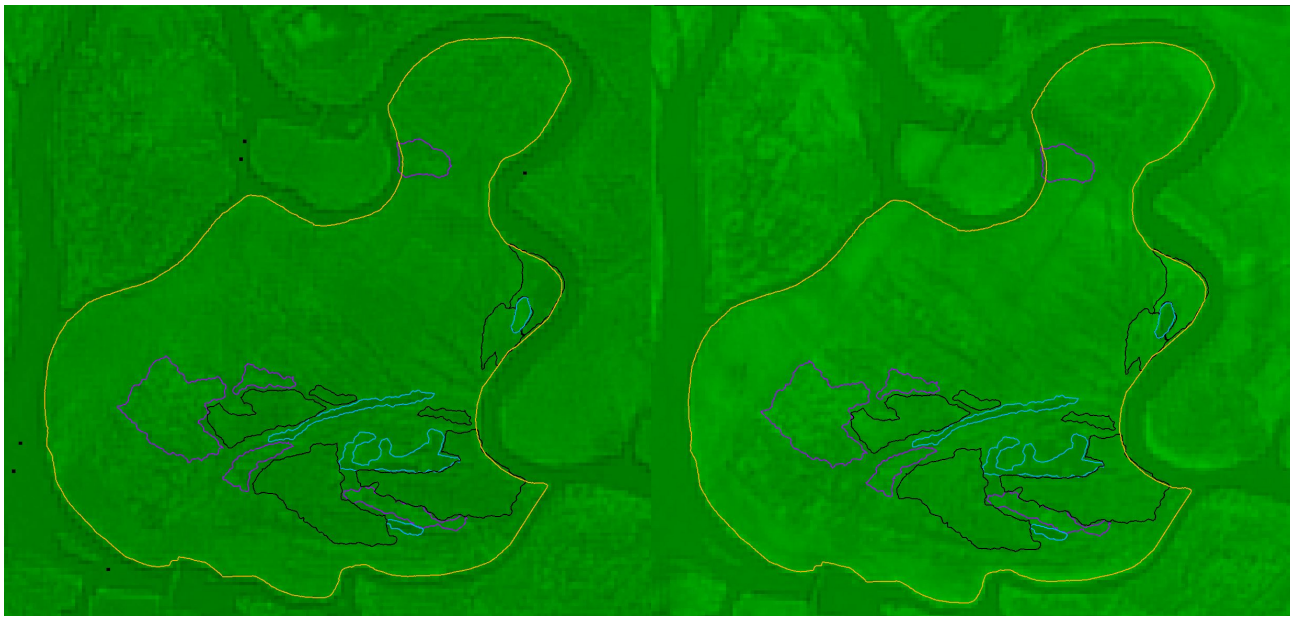

Figure 16: Gao's NDWI, computed from Sentinel-2 Level-2A data for two periods: December 13, 2022 (left) and March 17, 2024 (right). Purple polygons represent 91E0 Willow-poplar floodplain forests, black polygons represent Lk11 Reed beds, and blue polygons correspond to 3150 Natural eutrophic lakes with Magnopotamion or Hydrocharition-type vegetation.

5 Conclusion

We presented the hydrological modelling tool in the NaturaSat software and have shown its application in the case study of the Foráš Nature Reserve wetland in the alluvium of Danube River in Slovakia. By comparing the results of hydrological modelling with the Digital Terrain Model we studied waterlogging and health status of wetland habitats in the area. Usage of Sentinel-1 and Sentinel-2 satellite data further complemented the analysis. The findings underscore the potential of computational hydrological modelling, as it can represent an alternative to more time-consuming and costly in-field measurements. They demonstrate the value of integrating modern computational tools with environmental research to support sustainable wetland management and restoration.

Curve Name	December 13, 2022			March 17, 2024			Difference		
	Mean	Min	Max	Mean	Min	Max	Mean	Min	Max
curve_91E0_1	0.0747	-0.1031	0.2712	0.1820	-0.0010	0.3794	0.1073	0.1021	0.1082
curve_91E0_2	0.0647	-0.0775	0.1848	0.1744	0.0615	0.3195	0.1097	0.1390	0.1347
curve_91E0_3	0.0575	-0.0784	0.1768	0.1665	-0.0205	0.2730	0.1090	0.0579	0.0962
curve_91E0_4	0.0800	-0.0940	0.2059	0.1593	-0.0016	0.3130	0.0794	0.0924	0.1070
curve_91E0_5	0.0507	-0.0895	0.2000	0.1452	0.0302	0.2644	0.0946	0.1197	0.0644
curve_Lk11_1	0.0378	-0.0633	0.2308	0.2313	0.0671	0.4038	0.1936	0.1303	0.1730
curve_Lk11_2	0.0553	-0.0670	0.1995	0.1760	0.0011	0.4017	0.1207	0.0681	0.2022
curve_Lk11_3	0.0077	-0.1149	0.2295	0.1140	-0.0172	0.2476	0.1063	0.0977	0.0181
curve_Lk11_4	-0.0080	-0.0916	0.0955	0.1169	0.0055	0.2016	0.1249	0.0971	0.1061
curve_Lk11_5	0.0023	-0.1323	0.1889	0.1013	-0.0134	0.2398	0.0991	0.1194	0.0509
curve_Lk11_6	0.0072	-0.1074	0.1308	0.1203	-0.0185	0.3077	0.1131	0.0889	0.1768
curve_Lk11_7	0.0025	-0.0822	0.0860	0.1515	0.0793	0.2168	0.1490	0.1615	0.1308

Table 3: Statistical features (mean, minimum and maximum) computed for Gao's NDWI from Sentinel-2 data for two different periods, corresponding to segmented regions of the 91E0 Willow-poplar floodplain forests and Lk11 Reed beds habitats. Values are dimensionless.

Funding

This work was supported by European Space Agency contract 4000140486/23/NL/SC/rp "Monitoring of Slovakian wetlands with links to the Black Sea and Danube Regional Initiative", and by grants APVV-23-0186, APVV-22-0151 and VEGA 1/0249/24.

Author contributions

KM, MK and IP developed the mathematical and numerical model and computational hydrology tool, MS and JS suggested the case study, verified the habitats in the field and assessed the results, JP provided the data for boundary conditions in case of artificial flooding and contributed to data analysis and results interpretation.

Conflict of interest

The authors declare no conflict of interest.

References

[1] Algoritmy:SK, *NaturaSat*, Trial version, 2025. Available at: algoritmysk.eu

[2] M. Ambroz, M. Balažovjech, M. Medľa, K. Mikula, Numerical modeling of wildland surface fire propagation by evolving surface curves, *Advances in Computational Mathematics*, vol. 15, pp. 1067–1103, 2019. DOI: 10.1007/s10444-018-9650-4. Available at: link.springer.com.

[3] M. Ambroz, M. Kollár, K. Mikula, Semi-implicit scheme for semi-automatic segmentation in NaturaSat software, *Proceedings Of The Conference Algoritmy 2020*, pp. 171 - 180, 2020. Available at: iam.fmph.uniba.sk.

[4] CGAL Project, *CGAL User and Reference Manual*, CGAL Editorial Board, 6.0.1 edition, 2024. Available at: doc.cgal.org.

[5] N. C. Davidson, How Much Wetland Has the World Lost? Long-Term and Recent Trends in Global Wetland Area, *Marine and Freshwater Research*, vol. 65, no. 10, pp. 934–941, 2014. DOI: 10.1071/MF14173.

[6] Digital Terrain Model 6.0, *2nd project cycle (2022 – 2026) and creation of DTM 6.0*, Geodesy, Cartography and Cadastre Authority of the Slovak Republic (ÚGKK SR), 2024. Available at: web.archive.org.

[7] Digital Terrain Model 6.0, *Provision of ALS products*, Geodesy, Cartography and Cadastre Authority of the Slovak Republic (ÚGKK SR), 2024. Available at: web.archive.org.

[8] European Space Agency (ESA), *Sentinel Application Platform (SNAP)*, version 11.0.0, 2025. Available at: step.esa.int.

[9] European Space Agency (ESA), *Space key to wetland conservation*, `https://www.esa.int/Applications/Observing_the_Earth/Space_key_to_wetland_conservation`, Online; accessed February 2024.

[10] European Space Agency (ESA), *Copernicus Data Space Ecosystem*, Available at: dataspace.copernicus.eu.

[11] R. Eymard, T. Gallouët, R. Herbin, Finite volume methods, *Handbook of Numerical Analysis, Solution of Equation in Rn (Part 3), Techniques of Scientific Computing (Part 3)*, vol. 7, pp. 713-1018, 2000. DOI: 10.1016/S1570-8659(00)07005-8. Available at: sciencedirect.com.

[12] F. Filipponi, Sentinel-1 GRD Preprocessing Workflow, *Proceedings*, vol. 18, no. 1, p. 11, 2019. DOI: 10.3390/ECRS-3-06201. Available at: mdpi.com.

[13] B.C. Gao, NDWI - A normalized difference water index for remote sensing of vegetation liquid water from space, *Remote Sensing of Environment*, vol. 58, is. 3, pp. 257–266, 1996. DOI: 10.1016/S0034-4257(96)00067-3. Available at: sciencedirect.com.

[14] K. Mikula, J. Urbán, M. Kollár, M. Ambroz, I. Jarolímek, J. Šibík, and M. Šibíková, Semiautomatic segmentation of NATURA 2000 habitats in Sentinel-2 satellite images by evolving open curves, *Discrete and Continuous Dynamical Systems - S*, vol. 14, no. 3, pp. 1033–1046, 2021. DOI: 10.3934/dcdss.2020231. Available at: aimsciences.org.

[15] K. Mikula, J. Urbán, M. Kollár, M. Ambroz, I. Jarolímek, J. Šibík, and M. Šibíková, An automated segmentation of NATURA 2000 habitats from Sentinel-2 optical data, *Discrete and Continuous Dynamical Systems - S*, vol. 14, no. 3, pp. 1017–1032, 2021. DOI: 10.3934/dcdss.2020348. Available at: aimsciences.org.

[16] K. Mikula, M. Šibíková, M. Ambroz, M. Kollár, A. A. Ožvat, J. Urbán, I. Jarolímek, and J. Šibík, NaturaSat—A software tool for identification, monitoring and evaluation of habitats by remote sensing techniques, *Remote Sensing*, vol. 13, no. 17, article no. 3381, 2021. DOI: 10.3390/rs13173381. Available at: mdpi.com.

[17] K. Mikula, M. Kollár, A. A. Ožvat, M. Ambroz, L. Čahojová, I. Jarolímek, J. Šibík, and M. Šibíková, Natural numerical networks for Natura 2000 habitats classification by satellite images, *Applied Mathematical Modelling*, vol. 116, pp. 209–235, 2023. DOI: 10.1016/j.apm.2022.11.021. Available at: sciencedirect.com.

[18] K. Mikula, M. Kollár, A. A. Ožvat, M. Šibíková, and L. Čahojová, Natural numerical networks on directed graphs in satellite image classification, in *Scale Space and Variational Methods in Computer Vision*, L. Calatroni, M. Donatelli, S. Morigi, M. Prato, and M. Santacesaria, Eds., Springer International Publishing, Cham, 2023, pp. 339–351. ISBN: 978-3-031-31975-4. DOI: 10.1007/978-3-031-31975-4_26. Available at: springer.com.

[19] K. Mikula, M. Ambroz, and R. Mokošová, What was the river Ister in the time of Strabo? A mathematical approach, *Tatra Mountains Mathematical Publications*, vol. 80, issue. 3, 2021. DOI: 10.2478/tmmp-2021-0032. Available at: mat.savba.sk.

[20] K. Mikula, D. Ševčovič A direct method for solving an anisotropic mean curvature flow of plane curves with an external force, *Mathematical Methods in the Applied Sciences*, vol. 27, no. 13, pp. 1545-1565, 2004. DOI: 10.1002/mma.514. Available at: onlinelibrary.wiley.com.

[21] OpenStreetMap contributors, *Planet dump retrieved from* `https://planet.osm.org`, Available at: openstreetmap.org, 2024.

[22] Sentinel-1 Team, *Sentinel-1 User Handbook*, European Space Agency (ESA), Issue 1, Revision 0, 2013. GMES-S1OP-EOPG-TN-13-0001. Available at: sentinel.esa.int

[23] Sentinel-2 Team, *Sentinel-2 User Handbook*, European Space Agency (ESA), Issue 1, Revision 2, 2015. Available at: sentinel.esa.int

[24] The historical map of the First Military Survey, *Spatial Data Registry*, Ministry of the Environment of the Slovak Republic, 2024. Available at: rpi.gov.sk/en/.

[25] The historical map of the Second Military Surveys, *Spatial Data Registry*, Ministry of the Environment of the Slovak Republic, 2024. Available at: rpi.gov.sk/en/.

[26] The historical map of the Third Military Surveys, *Spatial Data Registry*, Ministry of the Environment of the Slovak Republic, 2024. Available at: rpi.gov.sk/en/.

Journal's webpage: http://univagora.ro/jour/index.php/ijccc/

This journal is a member of, and subscribes to the principles of,
the Committee on Publication Ethics (COPE).
https://publicationethics.org/members/international-journal-computers-communications-and-control

Cite this paper as:
Kollár, M.; Piačková, I.; Papčo, J.; Šibíková, M.; Šibík, J.; Mikula, K. (2025). NaturaSat computational tools for supporting hydrological modelling in environmental study and control, *International Journal of Computers Communications & Control*, 20(2), 7027, 2025.
https://doi.org/10.15837/ijccc.2025.2.7027